Applied Physics Letters ARTICLE scitation.org/journal/apl

Correlation between enhanced lattice distortion and volume fraction of polar nanoregions in quenched $Na_{1/2}Bi_{1/2}TiO_3$–$BaTiO_3$ ceramics

Cite as: Appl. Phys. Lett. **118**, 072903 (2021); doi: 10.1063/5.0039369
Submitted: 2 December 2020 · Accepted: 30 January 2021 ·
Published Online: 17 February 2021

Andreas Wohninsland,[a] Ann-Katrin Fetzer, Adeel Riaz, Hans-Joachim Kleebe, Jürgen Rödel, and Lalitha Kodumudi Venkataraman [a]

AFFILIATIONS

Department of Materials and Earth Sciences, Technical University of Darmstadt, 64287 Darmstadt, Germany

[a]Authors to whom correspondence should be addressed: wohninsland@ceramics.tu-darmstadt.de and venkataraman@ceramics.tu-darmstadt.de

ABSTRACT

Quenching has been established as a viable method to increase the depolarization temperature in (100-x) $Na_{1/2}Bi_{1/2}TiO_3$–$x$$BaTiO_3$ (NBT–xBT). The proposed hypothesis of a stabilized ferroelectric order would entail changes in the polarized volume. To this end, air-quenched and furnace cooled samples of four compositions of NBT–xBT with $x = 3$, 6, 9, and 12 mol. % BT were studied. Upon quenching, all the compositions demonstrate an increase in the ferroelectric to relaxor transition temperature, $T_{F\text{-}R}$, by 23–44 °C and enhanced lattice distortion. Resonance frequency damping analysis was utilized to measure Young's modulus in the temperature range of 25 °C to 800 °C and to estimate the volume fraction of polar nanoregions using a composite model. Quenching leads to an 8% decrease in Young's modulus, but to an increase in the volume fraction of polar nanoregions by 12% at 300 °C for NBT-6BT. Transmission electron microscopy investigations of quenched NBT-6BT reveal a combination of lamellar domains and more homogenous areas with nanometer-sized domains. The existence of lamellar domains in quenched morphotropic phase boundary compositions together with enhanced lattice distortion and a decrease in dielectric frequency dispersion substantiate the premise of a stabilized ferroelectric order.

Lead-free ferroelectrics[1,2] have made great progress in recent years accompanied by detailed investigations of their local structure. A pertinent lead-free nonergodic relaxor is the $Na_{1/2}Bi_{1/2}TiO_3$–$BaTiO_3$ (NBT–BT) solid solution with the morphotropic phase boundary (MPB) around 6 mol. % BT.[3,4] Dorcet and Trolliard[5] described nanometer-sized tetragonal platelets in a rhombohedral matrix in pure NBT, as residuals embedded in the high-temperature cubic phase. The polar nanoregions (PNRs) are 23 nm in size for compositions close to the MPB as reported by Zhang *et al.*,[6] which are in close agreement with the estimated correlation lengths of approximately 20 nm in NBT-4BT derived from diffuse x-ray scattering.[7] Utilizing transmission electron microscopy (TEM), Yao and co-authors[8] reported the PNRs to decrease in size when approaching the MPB in the NBT–BT system. For NBT-6BT, ^{23}Na nuclear magnetic resonance (NMR) established a polar volume fraction (VF) of 75% at room temperature.[9,10]

Recently, the thermal depolarization in relaxor NBT-based compositions has been correlated with the increased ferroelectric stability mediated by enhanced polarizability,[11,12] residual stress,[13] and off-centered Bi^{3+} displacement.[14] Quenching from sintering temperature is advantageous for increasing the thermal depolarization temperature with minimal departure in the electrical characteristics[15,16] and is demonstrated to be of practical relevance.[17] Previous works[14–16,18–20] indicate enhanced lattice distortion upon quenching, which plausibly results from the enhanced off-centering of Bi^{3+} along the polar direction. Such off-centering effects have also been reported earlier for furnace cooled (FC) specimens.[6,21] Off-centering of a positionally disordered cation along the polar direction is expected to enhance the lattice polarizability, stabilize a ferroelectric order, and, thus, also alter the volume fraction of PNRs. Understanding the structure property relationship for goal-oriented material tailoring would then involve knowledge of polar fractions, ideally as a function of temperature. The range of available methods to quantify phase fractions of the polarized volume in relaxors at elevated temperatures is limited, e.g., resonance frequency damping analysis (RFDA)[22] and NMR.[9,10]

This work contrasts a rhombohedral, tetragonal, and two MPB compositions of NBT–xBT to compare the volume fractions of PNRs

in the quenched state with those of a furnace cooled specimen. The propensity toward the ferroelectric state driven by the quenching treatment is further corroborated by the changes in lattice distortion and frequency dispersion in the dielectric permittivity.

Ceramic powders of (100-x)$Na_{1/2}Bi_{1/2}TiO_3$–$xBaTiO_3$, with $x = 3$, 6, 9, and 12 (here, x denotes mol. %), were synthesized via the solid state route.[15] After sieving, the calcined powder was pressed into cylindrical and rectangular shapes and sintered at 1150 °C for 3 h with a heating rate of 5 °C/min in a sacrificial powder of the respective composition and is referred to as FC (furnace cooled) sample. The quenched samples (referred to as Q) were taken out of the furnace directly after the sintering dwell time and cooled to room temperature assisted by a conventional air fan. Bar-shaped samples were ground from all sides to 30 × 4 × 3 mm^3, while cylindrical pellets were reduced to a thickness of 0.6 mm with a diameter of 10–11 mm. Annealing was performed at 400 °C for 30 min after the grinding step to relieve the induced stresses. Electrodes were applied to the pellets for electrical measurements with burnt-in silver paste. Poling was done in a silicon oil bath by applying a field of 6 kV/mm for 20 min.

Phase purity and lattice parameters were established by x-ray diffraction (on powders obtained from crushed pellets after annealing) performed using a Bruker D8 diffractometer in Bragg–Brentano geometry using Cu-K$\alpha_{1,2}$ radiation (Fig. S1 and Table SI in the supplementary material). Temperature and frequency-dependent permittivity measurements were carried out using an impedance analyzer (4192A LF, Hewlett-Packard) from room temperature to 500 °C with a heating rate of 2 °C/min on poled and unpoled samples. TEM investigations (2100F JOEL Ltd., Tokyo, Japan operated at 200 kV) were performed on samples prepared by standard ceramographic techniques including grinding, polishing, and Ar^+-ion milling. An additional annealing step at 400 °C for 30 min was included prior to ion milling, in order to relieve residual stresses introduced during grinding.

Young's modulus (Y) as a function of temperature on at least two different rectangular samples (Fig. S2 in the supplementary material) per composition was recorded using a resonance frequency and damping analyzer (RFDA-HT1750, IMCE, Genk, Belgium) from 25 to 800 °C with a heating rate of 2 °C/min.[22,23]

A composite model was used to calculate the volume fractions of PNRs from the evolution of Y with temperature.[24] It is based on the assumption of a two-phase mixture, consisting of a single phase, cubic matrix with spherical, tetragonal inclusions (PNRs) with different Young's moduli $Y_{cub}(T)$ and $Y_{tet}(T)$, respectively, while $Y_{cub}(T) > Y_{tet}(T)$.[22] Figure 1 details an exemplary measurement of Y(T) for NBT-12BT FC, which undergoes a phase transition from the normal ferroelectric to the relaxor at T_{F-R}. Below T_{F-R}, the material is tetragonal and the curve features a linear decrease in Y with increasing T. Upon further heating, the volume fraction of the cubic matrix phase increases, while the volume fraction of tetragonal inclusion decreases, resulting in an increase in Y. Therefore, the maximum in Y is associated with the transformation of the material into a pure cubic phase, followed by a linear decrease in Y with increasing T. The temperature at which Y reaches its maximum correlates with the Burns temperature T_B.[25] Applying linear fits in the low-temperature and high-temperature single phase regimes yields $Y_{tet}(T)$ and $Y_{cub}(T)$, respectively. This allows computation of the volume fraction of inclusions, in this case, PNRs.[24]

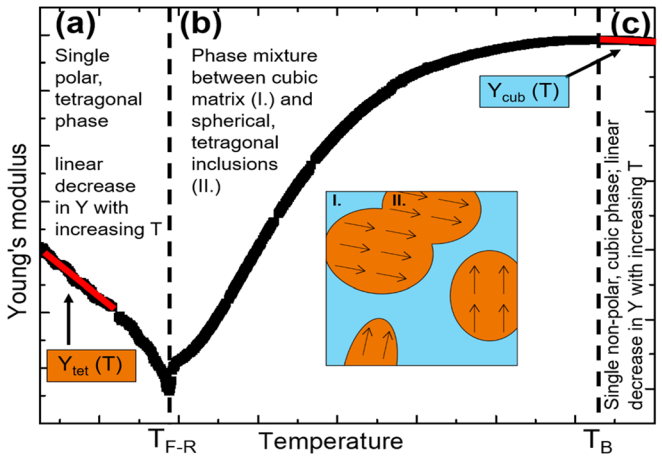

FIG. 1. Representative evolution of Young's modulus as a function of temperature for NBT-12BT FC with a phase transition from the normal ferroelectric (a) to the relaxor (b) and subsequently to the nonpolar cubic state (c).

Both NBT-3BT FC and Q exhibit a splitting of the 111_{pc} reflection along with a characteristic superlattice reflection (SR) at $2\theta \approx 38.3°$ indicating a rhombohedral structure (Fig. S1 in the supplementary material). NBT-6BT FC neither features peak splitting in 111_{pc} nor does it reveal a SR; therefore, a cubic model is used. The material exhibits weak rhombohedral distortions[26] using neutron diffraction; nevertheless, this could not be resolved with conventional laboratory XRD data used in this study. NBT-6BT Q, in contrast, indicates not only characteristics of a rhombohedral distortion including the SR, but also splitting in 200_{pc}, providing evidence of a mixture of tetragonal and rhombohedral phases. Tetragonal distortions are also visible in NBT-9BT Q and FC, but no SR was observed. Nevertheless, a pure tetragonal model did not result in a satisfactory fit, and hence, a mixture of tetragonal and rhombohedral phases was utilized.[13] For both NBT-12BT FC and Q, a tetragonal model was satisfactory to fit the data.

The lattice distortion is computed as 90-α and (c/a)-1 for the rhombohedral and tetragonal distortions, respectively (Fig. 2). Note

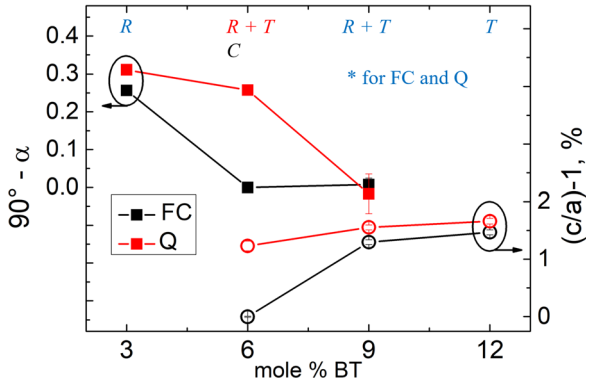

FIG. 2. Rhombohedral and tetragonal lattice distortions as a function of BT content derived from laboratory x-ray powder diffraction. The labels R, T, and C correspond to the crystal system-rhombohedral, tetragonal, and cubic, respectively.

that the distortions of Q are higher than FC for all the compositions and correlate with the increase in T_{F-R} upon quenching (Fig. S3 in the supplementary material) consistent with the literature.[15,18,19] However, the most significant changes in lattice distortion are noted for NBT-6BT. This is rationalized to be due to the onset of tetragonal distortion for NBT-6BT Q, which is absent in NBT-6BT FC.

Young's modulus and derived PNR volume fraction (VF) as a function of temperature in the unpoled state are plotted in Fig. 3. T_{F-R} and T_M are derived from dielectric measurements of poled FC and Q samples, respectively (Fig. S3 in the supplementary material). T_M corresponds to the temperature at which permittivity is maximum and does not deviate by more than 4% for FC and Q samples.

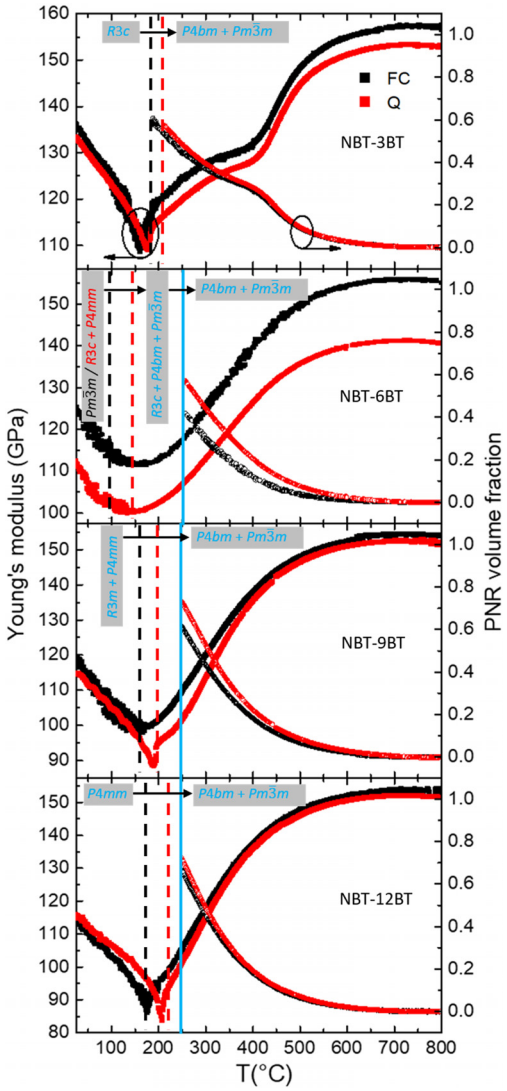

FIG. 3. Young's modulus and PNR volume fraction as a function of temperature for NBT-3, 6, 9, and 12BT. Vertical, dashed black and red lines denote T_{F-R}, and blue lines denote T_M [established from poled $\varepsilon'(T)$, Fig. S3 in the supplementary material] for FC and Q samples, respectively. The phase notations in blue correspond to the phase assemblage of furnace-cooled samples reported in the literature.[9,27,28]

Compositions with a linear decrease in Y upon heating and a sharp minimum in Y feature spontaneous ferroelectric behavior at low temperature, also evident in the absence of frequency dispersion in the dielectric measurements on unpoled samples.[15] While NBT-3BT and NBT-12BT feature sharp minima in Y regardless of FC or Q, this holds only for NBT-9BT Q but not for the FC sample. This provides additional evidence to a stabilization of the ferroelectric state upon quenching.

PNR VF as a function of composition at 300 °C is depicted in Fig. 4(a). At 300 °C, only tetragonal PNRs are assumed to be present. Quenching increases PNR VF especially for MPB compositions, NBT-6BT and NBT-9BT. The largest increase was obtained for NBT-6BT correlating with the largest increase in the lattice distortion for this composition (Fig. 2). At 300 °C, NBT-6BT FC exhibits a PNR VF of 31%, while NBT-6BT Q reveals 43% PNR VF. NBT-3BT and NBT-12BT, which are ferroelectrics at room temperature and more apart from the MPB, provide only marginal changes in PNR VF between FC and Q samples. Given that quenching is known to stabilize the ferroelectric order,[15] this warrants an increase in the coherence length of PNRs. The increase in the coherence length of PNRs would then involve an increase in the size of PNRs and/or an increase in their number density at higher temperatures; upon cooling, these polar

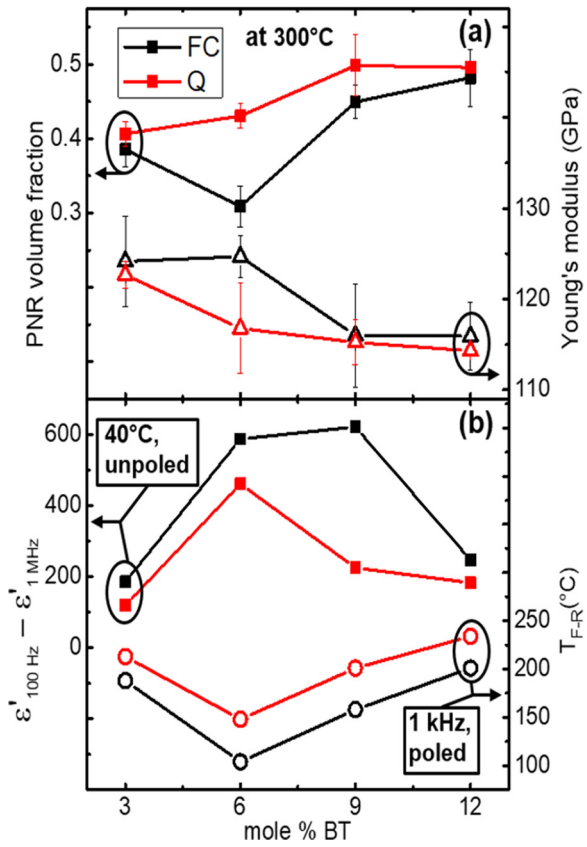

FIG. 4. (a) PNR volume fraction and Young's modulus as a function of BT content at 300 °C. (b) Difference in ε' of unpoled samples between low (100 Hz) and high (1 MHz) frequencies at 40 °C and T_{F-R} [established from the poled ε' (T), Fig. S3] as a function of BT content.

entities then coalesce into larger ferroelectric domains. Therefore, the increase in PNR VF at elevated temperatures promotes the ferroelectric order at room temperature. Note that above T_{F-R}, Q and FC of NBT-6BT and NBT-9BT exhibit a frequency dispersion in the dielectric response (clearly discerned from Fig. S4), characterizing the relaxor state. This, then rationalizes the increased PNR VF established for the quenched materials above T_{F-R}. Quenching NBT is known to result in a larger, but more consistent off-centering of the Bi^{3+}-ion, resulting in a more ordered local structure,[14] which can be linked to the stabilization of the ferroelectric state. Since Bi^{3+}-ion displacement induces the formation of PNRs, a correlation between the more pronounced off-centering and an increased PNR volume fraction is suggested.[6]

NBT-6BT exhibits the strongest decrease in Young's modulus (8%) upon quenching, consistent with the study by Zhang *et al.*,[17] and correlates with the strongest increase in lattice distortion. The other investigated compositions reveal only a marginal decrease in Y upon quenching. The decrease in Y caused by the quenching treatment is suggested to be related to the structural changes in the material, e.g., enhanced lattice distortion and larger off-centering of the Bi^{3+} ion.[17,18]

The difference in permittivity at low (100 Hz) and high (1 MHz) frequencies characterizes relaxor features[29] and is provided for unpoled samples at 40 °C in Fig. 4(b) (Fig. S4 in the supplementary material). Both FC and Q samples of NBT-3BT and NBT-12BT demonstrate the absence of frequency dispersion in permittivity at room temperature even in the unpoled state, while FC and Q samples of NBT-6BT feature relaxor characteristics. Q samples of all compositions exhibit lower values of $\varepsilon'_{100\,Hz}-\varepsilon'_{1\,MHz}$, compared to FC samples.

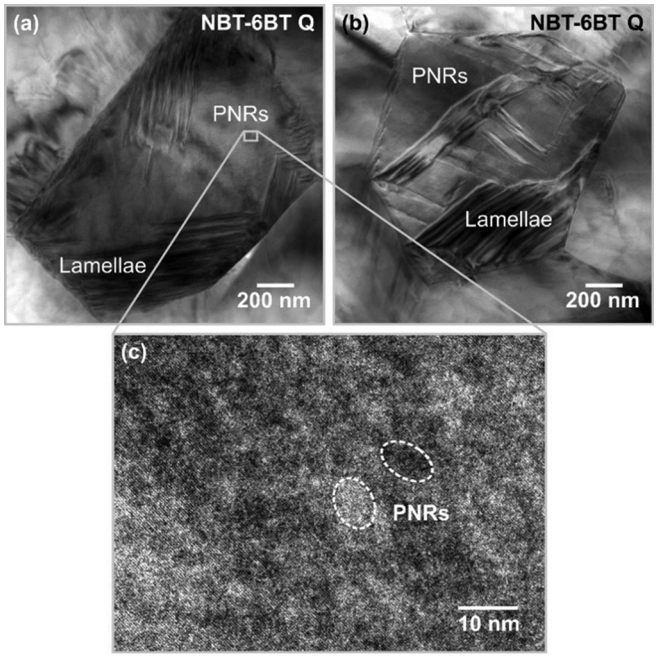

FIG. 5. TEM bright-field images of the NBT-6BT Q sample. In (a) and (b), one grain is displayed, each showing lamellar domain structures next to areas of more homogeneous contrast without lamellae. The latter exhibit a grainy contrast variation on the nanometer scale, displayed in (c), attributed to the PNR nanostructure.

A strong difference in $\varepsilon'_{100\,Hz}-\varepsilon'_{1\,MHz}$ can be observed for FC and Q samples of NBT-9BT, validating the stabilization of the ferroelectric state upon quenching. These observations correlate with the results from RFDA measurements. Temperature-dependent dielectric data from poled samples (Fig. S3 in the supplementary material) reveal an increase in T_{F-R} by 23–44 °C upon quenching [Fig. 4(b)], which is consistent with reported values.[15,30]

The domain structure is exemplarily investigated for quenched NBT-6BT, which exhibited the highest increase in PNR VF [Figs. 5(a) and 5(b)]. TEM bright-field images of unpoled NBT-6BT Q reveal lamellar domains next to areas with a more homogenous contrast [Figs. 5(a) and 5(b)]. In regions where no lamellar domains appear, a grainy contrast is visible on a magnified scale [Fig. 5(c)]. Here, the small regions exhibiting a variation of brighter and darker contrast can be attributed to the PNR nanostructure. They are in the size range of approximately 5 to 10 nm. The presence of areas with lamellar domain contrast reflects the increased coherence length between the PNRs and consequently increased lattice distortion upon quenching.

To summarize, an increase in the volume fraction of PNRs is evidenced for quenched NBT–*x*BT, with a pronounced difference of 12% noted for the MPB composition, NBT-6BT. The non-MPB compositions exhibit negligible changes in PNR VF due to their innate non-cubic distortions as opposed to NBT-6BT. These results are correlated with an increased lattice distortion upon quenching and reinforce the proposed stabilization of the ferroelectric state.

See the supplementary material for the diffraction patterns (Fig. S1) and lattice parameters (Table SI) of furnace cooled and quenched samples, comparison of RFDA measurements of three different NBT-6BT FC samples (Fig. S2), and temperature-dependent real and imaginary part of the permittivity of poled and unpoled samples (Figs. S3 and S4).

L.K.V., H.J.K., A.W., and A.K.F. thank the Deutsche Forschungsgemeinschaft (DFG) for financial support under Nos. KO 5948/1-1 and KL 615/34-1 (Grant No. 414311761). A.W. thanks Patrick Breckner for enabling the operation and maintenance of the RFDA equipment and writing a data evaluation program and Michael Scherer for improving crucial parts of the measurement setup.

DATA AVAILABILITY

The data that support the findings of this study are available within this article and its supplementary material.

REFERENCES

[1]A. J. Bell and O. Deubzer, MRS Bull. **43**, 581 (2018).
[2]J. Koruza, A. J. Bell, T. Frömling, K. G. Webber, K. Wang, and J. Rödel, Materiomics **4**, 13 (2018).
[3]T. Takenaka, K. Maruyama, and K. Sakata, Jpn. J. Appl. Phys., Part 1 **30**, 2236 (1991).
[4]T. Tou, Y. Hamaguti, Y. Maida, H. Yamamori, K. Takahashi, and Y. Terashima, Jpn. J. Appl. Phys., Part 1 **48**, 07GM03 (2009).
[5]V. Dorcet and G. Trolliard, Acta Mater. **56**, 1753 (2008).
[6]H. W. Zhang, G. C. Deng, A. J. Studer, X. B. Li, X. Y. Zhao, and H. S. Luo, Scr. Mater. **86**, 5 (2014).
[7]J. E. Daniels, W. Jo, J. Rodel, D. Rytz, and W. Donner, Appl. Phys. Lett. **98**, 252904 (2011).

[8]J. J. Yao, N. Monsegue, M. Murayama, W. N. Leng, W. T. Reynolds, Q. H. Zhang, H. S. Luo, J. F. Li, W. W. Ge, and D. Viehland, Appl. Phys. Lett. **100**, 012901 (2012).
[9]P. B. Groszewicz, H. Breitzke, R. Dittmer, E. Sapper, W. Jo, G. Buntkowsky, and J. Rödel, Phys. Rev. B **90**, 220104(R) (2014).
[10]P. B. Groszewicz, M. Gröting, H. Breitzke, W. Jo, K. Albe, G. Buntkowsky, and J. Rödel, Sci. Rep. **6**, 31739 (2016).
[11]L. Li, M. K. Zhu, K. L. Zhou, Q. M. Wei, M. P. Zheng, and Y. D. Hou, J. Appl. Phys. **122**, 204104 (2017).
[12]L. Kodumudi Venkataraman, T. Zhu, M. Pinto Salazar, K. Hofmann, A. I. Waidha, J. C. Jaud, P. B. Groszewicz, and J. Rödel, J. Am. Ceram. Soc. (published online 2020).
[13]L. Kodumudi Venkataraman, M. Hinterstein, K.-Y. Lee, T. Yang, L.-Q. Chen, P. B. Groszewicz, J. Koruza, and J. Rödel, Phys. Rev. B **101**, 174108 (2020).
[14]H. Nagata, Y. Takagi, Y. Yoneda, and T. Takenaka, Appl. Phys. Express **13**, 061002 (2020).
[15]L. Kodumudi Venkataraman, J. Koruza, and J. Rödel, Appl. Phys. Lett. **113**, 252902 (2018).
[16]K. Eguchi, Y. Takagi, H. Nagata, and T. Takenaka, Jpn. J. Appl. Phys., Part 1 **59**, SPPD03 (2020).
[17]M. H. Zhang, P. Breckner, T. Frömling, J. Rödel, and L. Kodumudi Venkataraman, Appl. Phys. Lett. **116**, 262902 (2020).
[18]H. Muramatsu, H. Nagata, and T. Takenaka, Jpn. J. Appl. Phys., Part 1 **55**, 10tb07 (2016).
[19]T. Miura, H. Nagata, and T. Takenaka, Jpn. J. Appl. Phys., Part 1 **56**, 10pd05 (2017).
[20]P. R. Ren, J. L. Wang, Y. K. Wang, L. Kodumudi Venkataraman, and G. Y. Zhao, J. Eur. Ceram. Soc. **40**, 2964 (2020).
[21]E. Aksel, J. S. Forrester, J. C. Nino, K. Page, D. P. Shoemaker, and J. L. Jones, Phys. Rev. B **87**, 104113 (2013).
[22]M. Vögler, N. Novak, F. H. Schader, and J. Rödel, Phys. Rev. B **95**, 024104 (2017).
[23]ASTM E1876-99, "Standard test method for dynamic Young's modulus, shear modulus, and Poisson's ratio by impulse excitation of vibration" (ASTM International, West Conshohocken, PA, 2001).
[24]G. J. Weng, Int. J. Eng. Sci. **22**, 845 (1984).
[25]M. A. Carpenter, J. F. J. Bryson, G. Catalan, and C. J. Howard, J. Phys. **24**, 045901 (2012).
[26]R. Garg, B. Narayana Rao, A. Senyshyn, and R. Ranjan, J. Appl. Phys. **114**(23), 234102 (2013).
[27]B. N. Rao, M. Avdeev, B. Kennedy, and R. Ranjan, Phys. Rev. B **92**, 214107 (2015).
[28]C. Ma and X. Tan, J. Am. Ceram. Soc. **94**, 4040 (2011).
[29]F. Li, S. Zhang, D. Damjanovic, L.-Q. Chen, and T. R. Shrout, Adv. Funct. Mater. **28**, 1801504 (2018).
[30]Z. T. Li, H. Liu, H. C. Thong, Z. Xu, M. H. Zhang, J. Yin, J. F. Li, K. Wang, and J. Chen, Adv. Electron. Mater. **5**, 1800756 (2019).